INTERPRETATION OF IMPACT CRATER MORPHOLOGY AND RESIDUES ON LDEF USING 3-D SPACE DEBRIS AND MICROMETEOROID MODELS.

N.G. Mackay, S.F. Green, S.P. Deshpande, P.J. Newman.

Unit for Space Sciences, University of Kent, Canterbury, Kent CT2 7NR, U.K.

ABSTRACT

Study of the morphology of individual impact craters on surfaces of the Long Duration Exposure Facility provides a method for determination of the direction of the impacting particle. We describe the classification of craters suitable for such a study, models of the interplanetary and space debris directional fluxes for their interpretation, and present some results for surfaces on the Space face of LDEF. A significant unidentified source of particles producing elliptical craters with apparent trajectories from the Earth direction is apparent. Oblique impacts on the Space and Earth faces provide the best discrimination between debris in low and high eccentricity orbits.

1. INTRODUCTION

Interpretation of the wealth of impact data available from the Long Duration Exposure Facility, in terms of the absolute and relative populations of space debris and natural micrometeoroids, requires three dimensional models of the distribution of impact directions, velocities and masses of such particles. Although LDEF was in a gravity-gradient stabilised orbit with its long axis nominally pointing along the radius vector and one face (East) along the orbital velocity vector, a small tilt and offset from this geometry occurred. Thus, every face of LDEF was potentially exposed to micrometeorites and debris (even those in circular orbits) in varying proportions. Interpretation of these data requires models of the IP and space debris particle size and velocity distributions *as well as* the conversion from crater or foil perforation statistics to particle parameters. The models (refs. 1, 2) use the known properties of the debris or micrometeoroid populations to determine the geocentric velocity and spatial density fields, through which the spacecraft (LDEF) orbits. The relative impact velocities and fluxes are determined for each defined face of the polygonal spacecraft, from which the crater size distribution and foil perforation counts are modelled. The space debris population is represented by ~6700 orbits and a size distribution modelled from fits to in-situ data and known debris objects. The micrometeoroid population is represented by a geocentric isotropic flux derived from interplanetary measurements using a meteor velocity distribution.

The stabilised orbit of LDEF provides limited directional information from the fluxes on each face, but it is possible to determine more accurate impact directions from detailed crater morphology (ref. 3). Impacts at large angles of incidence and relatively low velocity produce craters which are elongated along the direction of impact with characteristic shapes from which the direction may be determined. The degree of ellipticity is dependent on the velocity, angle of incidence, and probably the particle and target materials.

In a previous paper (ref. 3) we presented a demonstration of the technique, and preliminary results for a few impacts. The model output was represented by a measure of the "total ellipticity" for particles impacting from a given azimuthal direction for comparison with directions of observed craters. We present here a more direct comparison between directional fluxes from the models and derived impact directions from elliptical craters, together with some new results from the South face of LDEF.

Further evidence of the source of impacting particles is obtained from the elemental composition of chemical residues. Kessler, (ref. 4) suggests an excess of debris in high eccentricity orbits at certain inclinations to explain the ratio of man-made particles on the North and West (trailing) faces. We use our models to comment on the best way of distinguishing such objects on other faces of LDEF.

2. ELLIPTICAL IMPACT CRATERS

2.1. Crater Morphology

Any smooth exposed surface is suitable for searches for elliptical craters using the Unit's Philips 525M scanning electron microscope. Images of each impact site are taken from normal to the clamp surface and at ± 7.5° to the normal. The two off-axis images are examined using a stereo viewer, enabling positive identification of true hypervelocity impacts sites. The stereo reconstructions of these impacts allow the depth and the maximum and minimum diameter of each crater to be measured, using the plane of the surface as a reference point. For "elliptical" craters, an estimate of the direction of impact can also be made using criteria obtained from experimental impact studies at oblique angles. Such impacts form elliptical craters with high raised lips on the side from which the impact occurred (the entrance side) and flattened lips on the exit side. The crater walls are steeper and sometimes undercut on the entrance

side. The shape of the crater is not truly elliptical, but egg-shaped, being deeper and wider at the entrance side (refs. 5, 6) (see figure 2). "Ellipticity" used here is determined from the major and minor axes, a and b

$$e = (1 - b^2/a^2)^{1/2} \qquad (1)$$

Craters on LDEF surfaces have been placed in three categories:

"Circular" - Irregularities in the surface and uncertainties in the exact crater edge result in ellipticities smaller than 0.3 being indistinguishable from circular.

"Elliptical" - Craters with morphology characteristic of oblique impacts. The direction of impact can be estimated with an accuracy of approximately 20 degrees

"Undefined" - Craters with elliptical shapes but unusual morphology. It is not possible to determine which was the entrance or exit side or even if the crater was the result of an oblique impact. Such craters could be produced by low velocity irregularly shaped or heterogeneous particles.

Representative craters are illustrated in figures 1-3.

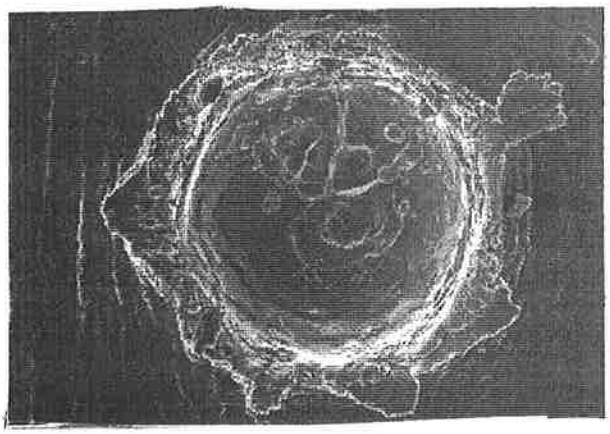

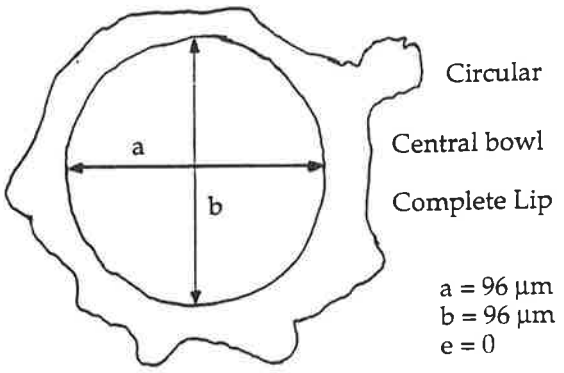

Figure 1. A crater classified as "circular" detected on a South face clamp from LDEF.

2.2. Data sources

The aluminium clamps used to support each experiment tray provide suitable surfaces for study of elliptical craters since they are available for all faces on LDEF. We present here data for a scanned area of 27cm^2 of a clamp from the South face resulting in identification of 26 circular, 31 elliptical and 50 undefined craters . The smallest identified crater is of diameter 2μm although sampling is complete only to a diameter of 4μm due to SEM resolution and clamp surface roughness. This is a somewhat higher resolution than the previous survey (ref. 3) and represents the limit of applicability for clamp surfaces. The technique is applicable to smaller craters on prepared surfaces such as the foils of the Micro-Abrasion Package (MAP) experiment on LDEF.

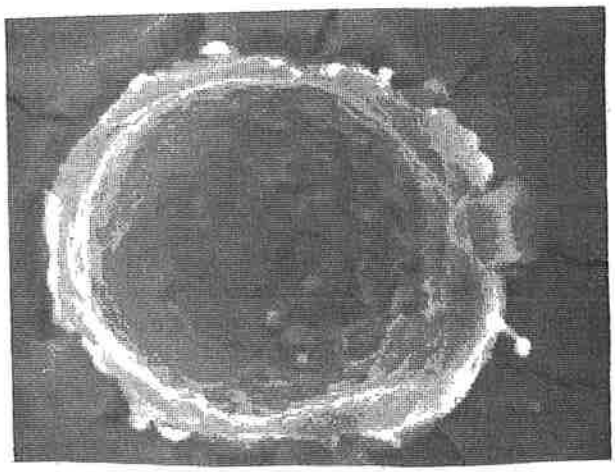

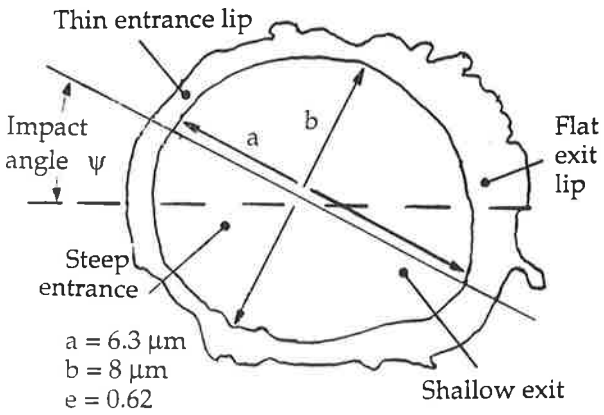

Figure 2. A crater classified as "elliptical" detected on a South face clamp from LDEF.

2.3. Derivation of impact angle

Impact experiments into metals (eg ref. 5) indicate that craters are circular for impact angles up to a critical angle, above which they exhibit the properties described above (ref. 6). As the particle velocity is increased, the critical angle increases (ref. 7). For material with no cohesive strength, the critical angle is large (>60° from the normal) and dependent on velocity and physical properties of the target and projectile (ref. 8). These experimental results apply to a range of materials and velocity and impact angle regimes but the relationship

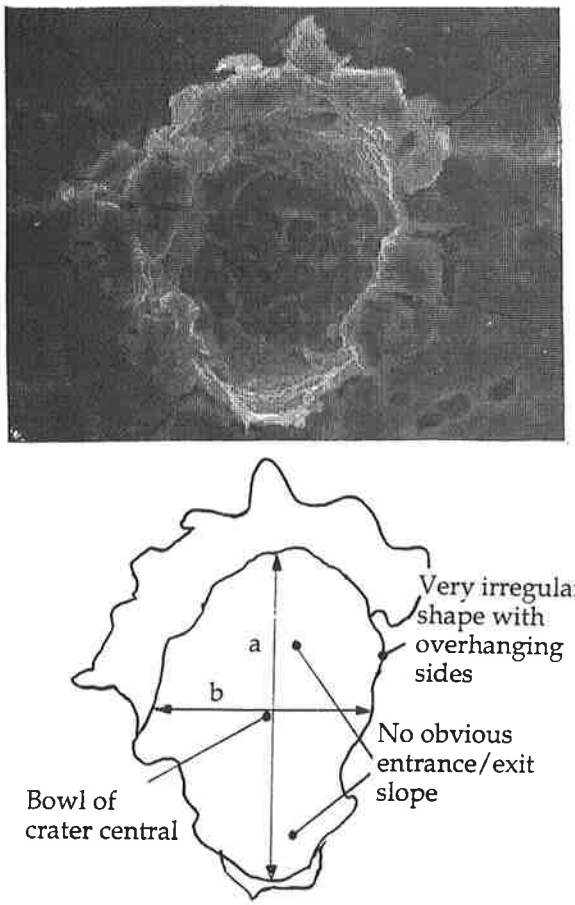

Figure 3. A crater classified as "undefined" detected on a South face clamp from LDEF.

between crater ellipticity and such properties is not well quantified. For this analysis we have adopted a simple relationship between impact angle and ellipticity, independent of impact velocity and particle properties (figure 4). Although this is physically un-realistic, a more sophisticated approach is not yet possible, and trends in the data are still easily identifiable.

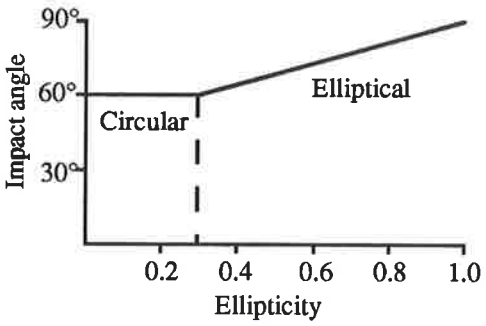

Figure 4. Simple relationship between crater ellipticity and angle of incidence adopted for this analysis.

Much of the experimental data have been obtained in relatively low velocity regimes which favour non-circular crater production, whereas typical velocities in space are considerable larger. However, a significant number of craters on LDEF are non-circular and therefore contain information on the direction of impact.

One would intuitively expect space debris impacts, which occur at lower velocities than interplanetary particles, to produce a larger fraction of the elliptical craters than of the total number of impacts.

Figure 5 illustrates the South clamp data analysed so far in a three dimensional diagram representing azimuthal and incidence angles and particle flux.

3. INTERPLANETARY DUST AND SPACE DEBRIS MODELS

3.1. Model structure

For each population (debris and Interplanetary) the numbers, and velocities of particles as a function of geocentric direction are determined. For a spacecraft of given orbital altitude and inclination the resultant impact fluxes and velocities are calculated, from which the fluxes on each spacecraft face are derived. Empirical relationships to convert particle properties to crater morphology are then applied to produce a crater (or foil perforation) size distribution

3.2. Spacecraft geometry

The time averaged orbital altitude of LDEF was 460 km yielding an orbital velocity of 7.64 km s^{-1}. LDEF was a 12 sided cylinder with face 9 (East) nominally pointing towards the velocity vector (ram direction) and the central axis aligned with the radius vector. Post-recovery analysis indicates a true attitude with an offset (rotation about the central axis such that the North face (12) points slightly towards the ram direction and the South face (3) slightly away from it) of 8° and a tilt of the space end towards the ram direction of 1.1°.

3.3. Space debris

The space debris population is described by the orbits of known debris objects extracted from the ESA DISCOS database (ref. 9) with the assumptions:

1) known debris orbits are representative of the total population;
2) longitudes of the nodes are random;
3) lines of apsides are random;
4) orbit distribution is constant with debris size.

The model results should be regarded as average values rather than valid for any particular time or exact location. Debris with large surface area to mass ratios suffer greater perturbations due to airdrag in LEO, so are likely to have different orbital distributions. Eccentric orbits are likely to be under-represented by the model since they are only in LEO for a small percentage of their orbital periods. The size distribution from the model by Kessler et al (ref. 10) is for impact fluxes and so cannot be deconvolved to space densities without a knowledge of the impact velocity distribution. Therefore the shape of this size distribution (which does not differ significantly with inclination or altitude above 200 km) has been used with a normalisation to the total numbers of catalogued objects in LEO at the largest sizes

where observational selection effects are negligible. A density of 2.8 g.cm^{-3} is assumed for space debris.

3.4. Interplanetary dust

The interplanetary dust particles are assumed to have an isotropic geocentric flux distribution with speeds at an altitude of 100 km determined from meteor data at constant mass (ref. 11) corrected for gravitational acceleration to an altitude of 460 km. At LDEF's altitude, Earth shielding removes particles from directions originating in a cone of semi-angle 73° from the Earth direction. An effective atmospheric altitude of 150 km is assumed. The size dependent geocentric flux of IP particles is derived from the interplanetary flux (as a function of mass) (ref. 12) assuming spherical particles of density 1000 kg m^{-3} and scaled by a gravitational enhancement factor G of 1.7 (from $G=1+0.76(r_e/r)$, where r_e = Earth's radius and r = geocentric distance of the spacecraft orbit, ref. 13).

3.5. Impact equations

In order to convert from impact fluxes as a function of particle size to number of craters as a function of crater diameter, the following empirically derived relationships (ref. 14) are used:

$$f = 0.6d\,(\rho_p/\rho_T)^{0.26}\,(\sigma_T/\sigma_o)^{-0.08}\,V^{\beta} \quad (2)$$

$$\beta = 0.69\,(\rho_p/\rho_T)^{0.09} \quad (3)$$

$$D_h = f/0.75 \quad (4)$$

where particle diamater = d, particle velocity = V, particle density = ρ_p, target density = ρ_T, target tensile strength = σ_T, the tensile strength of aluminium = σ_o (80 MPa), the thickness of foil that will just be perforated = f, and crater diameter = D_h.

4. INTERPRETATION OF ELLIPTICAL CRATER DATA

Figures 5-13 illustrate the data for the South face clamp and models for a number of faces showing impact azimuthal and incidence angles and fluxes, The models are calculated for impacts into aluminium with fluxes derived at a crater diameter of 4μm or larger. The predicted fluxes are in general agreement with the observed crater counts but detailed comparison of the relative numbers of space debris and interplanetary dust is not possible *directly* from the models due to the uncertainty in the input parameters, in particular the total populations. The following results are apparent:

- South face:
  - The interplanetary dust impacts (figure 6) are predominantly from the Space and East directions as would be expected from LDEF's orbital motion and Earth shielding. There are a significant number of highly oblique impacts in this quadrant which may produce elliptical craters despite the high impact velocity.
  - The space debris model (figure 7) predicts impacts only from directions close to the East (Ram) direction at angles of incidence dependent on the inclination of the debris orbit with respect to LDEF's orbit plane. The lower velocity of space debris implies a possible source of elliptical craters in the East direction.
  - The measured Space face data (figure 5) show a concentration in the East direction as would be expected for debris, but also a large number striking from the Earth direction.
  - Figure 8 illustrates the effect of increasing the number of debris objects in highly eccentric orbits by a factor of 20, as suggested by Kessler (ref. 4) to explain the large number of space debris impacts

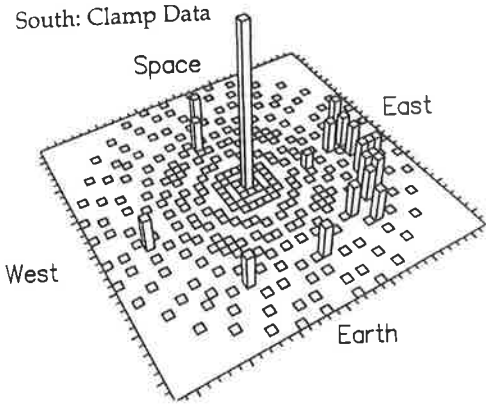

Figure 5. Elliptical crater data from an LDEF experimental tray clamp from the South face. Radial distance from the centre of the plot represents impact incidence angle, with the azimuthal directions indicated with respect to other LDEF pointing directions. The height of each column represents the flux. The central peak contains all craters with elliptical characteristics but with ellipticities smaller than the nominal measurable limit of 0.3. These data can be compared with model predictions shown in figures 6-8.
Flux scale $0 \rightarrow 1045 \times 10^{-8}$ m^{-2} s^{-1}

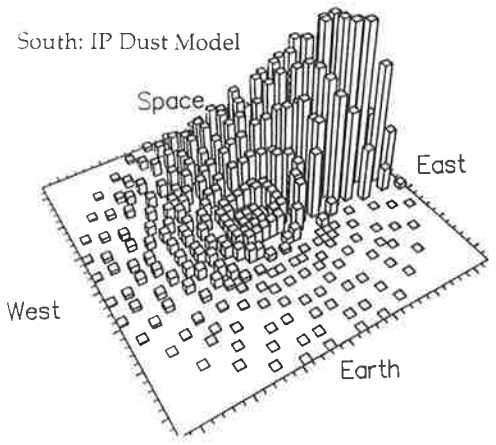

Figure 6. Predicted directional flux distribution for interplanetary dust on the South face of LDEF. Radial distance from the centre of the plot represents impact incidence angle, with the azimuthal directions indicated with respect to other LDEF pointing directions. The height of each column represents the flux.
Flux scale $0 \rightarrow 110 \times 10^{-8}$ m^{-2} s^{-1}

found from chemical residues on the West face. Such objects clearly are not sufficient to explain the source of observed elliptical craters.

- West Face:
  - The predicted interplanetary fluxes (figure 9) are

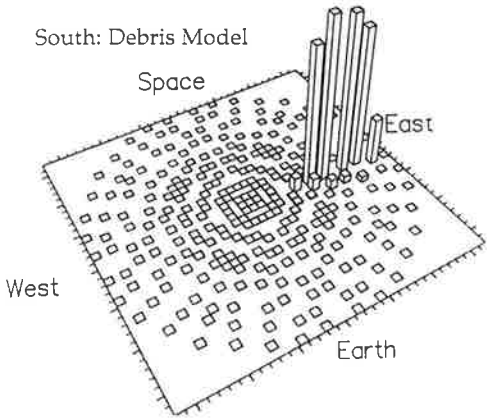

Figure 7. As figure 6 but for space debris on the South face of LDEF. Flux scale $0 \rightarrow 2750 \times 10^{-8}$ m^{-2} s^{-1}

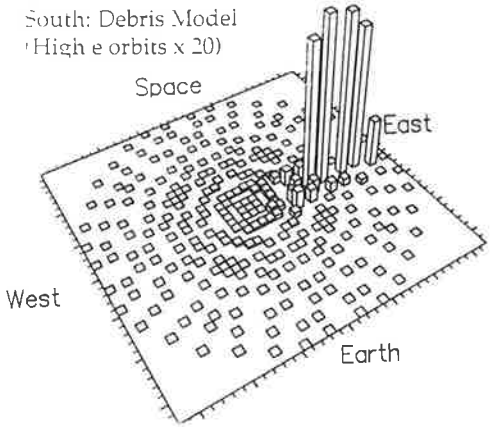

Figure 8. As figure 6 but for space debris with high eccentricity orbits increased by a factor of 20, on the South face of LDEF. Flux scale $0 \rightarrow 2750 \times 10^{-8}$ m^{-2} s^{-1}

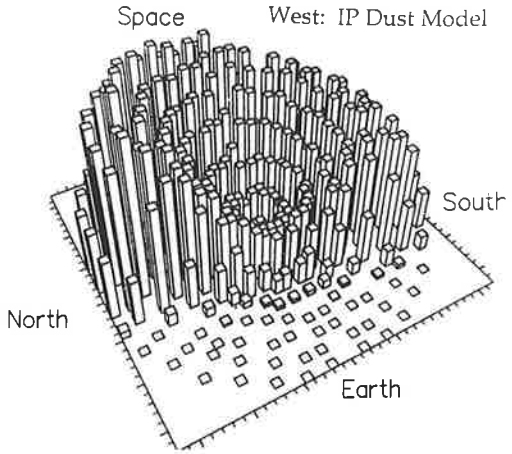

Figure 9. As figure 6 but for interplanetary dust on the West face of LDEF. Flux scale $0 \rightarrow 11 \times 10^{-8}$ m^{-2} s^{-1} significantly higher than those predicted for debris (figure 10) although the impact velocities are also higher. However, almost all the debris impacts are from objects in highly eccentric orbits, so if the population is indeed 20 times larger, they are still likely to dominate the elliptical crater population.

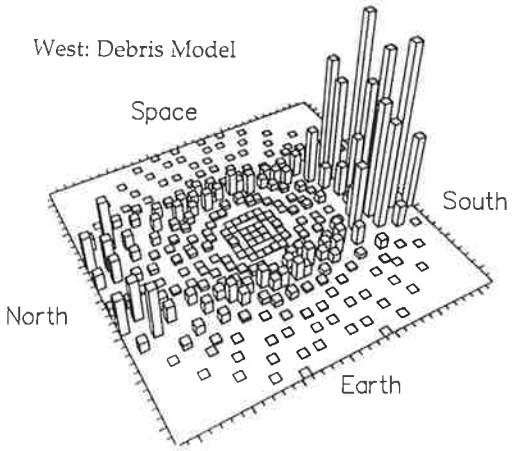

Figure 10. As figure 6 but for space debris on the West face of LDEF. Flux scale $0 \rightarrow 2.2 \times 10^{-8}$ m^{-2} s^{-1}

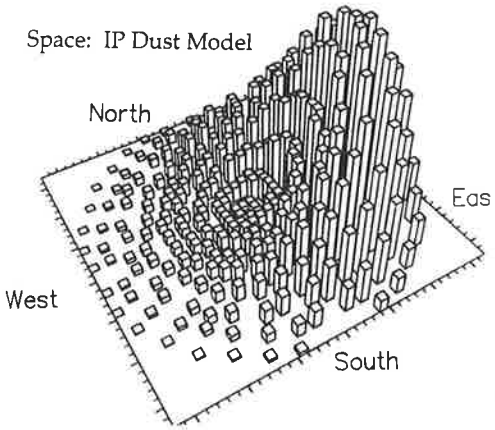

Figure 11. As figure 6 but for interplanetary dust on the Space face of LDEF. Flux scale $0 \rightarrow 165 \times 10^{-8}$ m^{-2} s^{-1}

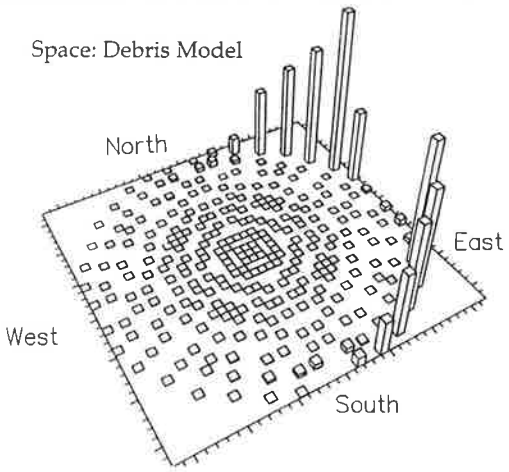

Figure 12. As figure 6 but for space debris on the Space face of LDEF. Flux scale $0 \rightarrow 110 \times 10^{-8}$ m^{-2} s^{-1}

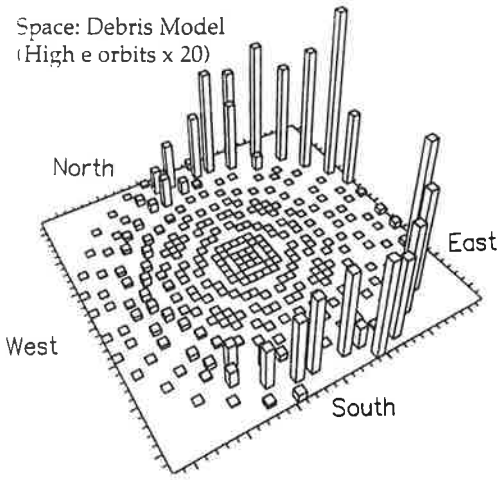

Figure 13. As figure 6 but for space debris with high eccentricity orbits increased by a factor of 20, on the Space face of LDEF. Flux scale $0 \rightarrow 110 \times 10^{-8}$ m^{-2} s^{-1}

- Space Face:
  - The interplanetary model predicts impacts predominantly from the East direction due to LDEF's orbital motion (figure 11).
  - The space debris impacts (figure 12) only occur at highly oblique angles from the North-East and South-East directions. The space face is just accessible to debris in circular orbits due to the 1.1° tilt of LDEF towards the Ram direction. Debris in highly eccentric orbits have impact directions from North and South. Elliptical crater data from the Space face can therefore be used to determine the relative numbers of objects in highly eccentric orbits.
  - The same pattern emerges on the Earth face, with the added advantage of less potential contamination from interplanetary particles.

The value of this type of analysis is apparent from the results presented here. We intend to survey clamps and foils over a large size range from a number of LDEF faces, but the location of impact sites, particularly on the West face requires high resolution scanning of large areas to identify a significant number of craters. The relationship between eccentricity of an impact crater, angle of impact, velocity and other factors is currently being determined using the Unit's 2MV Van der Graaff electrostatic accelerator.

5. ACKNOWLEDGEMENTS

We acknowledge the financial support of the UK Science and Engineering Research Council.

6. REFERENCES

1. Green, S.F. and McDonnell, J.A.M.M., 1992. A numerical model for characterisation of the orbital debris environment. In "Hypervelocity Impacts in Space", proceedings of workshop, University of Kent, 1-5 July 1991, (Ed. J.A.M. McDonnell), 251-256.

2. Green, S.F., Deshpande, S.P. and Mackay, N.G., 1993. A 3-D numerical model for space debris and interplanetary dust fluxes incident on LDEF. *Adv. Space Res.*, in press.

3. Newman P.J., Mackay N., Deshpande S.P., Green S.F. and McDonnell J.A.M., 1993. Derivation of Particulate Directional Information from Analysis of Elliptical Impact Craters. *Proc. Second LDEF Post-retrieval Conference.*, in press.

4. Kessler, D.J., 1992. Origin of orbital debris impacts on LDEF's trailing surfaces. NASA Johnson Space Center.

5. Kineke, J.H. Jr., 1960. An Experimental Study of Crater Formation in Metallic Targets. Hypervelocity Impact, 4th Symposium, Air Proving ground Center, Eglin Air Force Base Florida, APGC-TR-60-39 (I), section 4.

6. Bryan, G.M., 1960. A Model of Oblique Impact. Hypervelocity Impact, 4th Symposium, Air Proving ground Center, Eglin Air Force Base Florida, APGC-TR-60-39 (III), section 33.

7. Culp, F.L., 1959. Volume-Energy Relation for Craters Formed by High-Velocity Projectiles. Hypervelocity Impact, 3rd Symposium, Armour Research Foundation of Illinois Inst. of Technology, Chicago.

8. Gault, D.E. and Wedekind, J.A., 1978. Experimental Studies of Oblique Impact. *Proc. 9th Lunar Planet Sci. Conf.*, 3843-3875.

9. Klinkrad, H., Fuller, U., Searle, J. and Zarnecki, J.C., 1991. Retrieval of space debris information from ESA's DISCOS catalogue. *Proc. ESA workshop on space environment analysis*, 9-12 October 1990, ESTEC. ESA WPP-23 section 2.6.

10. Kessler, D.J., Reynolds, R.C., and Anz-Meador, P.D. 1989. Orbital Debris Environment for Spacecraft Designed to Operate in Low Earth Orbit, NASA TM 100471.

11. Erickson, J.E., 1968. Velocity Distribution of Sporadic Photographic Meteors. *Journal of Geophysical Research* 73 (12) 3721-3726.

12. Grün, E., Zook, H.A., Fechtig, H. and Giese, R.H., 1985. Collisional Balance of the Meteoric Complex. *Icarus* 62, 244-272

13. NASA, 1970. Meteoroid Environment Model - 1970 (Interplanetary and Planetary). NASA Space Vehicle Design Criteria (Environment). NASA SP-8038.

14. McDonnell, J.A.M., Deshpande, S.P., Green, S.F., Newman, P.J., Paley, M.T., Ratcliff, P.R., Stevenson, T.J. and Sullivan, K., 1991. First Results Of Particulate Impacts And Foil Perforations On LDEF. *Advances In Space Research* 11, (12)109-(12)114.